FLiER: Practical Topology Update Detection Using Sparse PMUs

Colin Ponce and David S. Bindel

Abstract—**In this paper, we present a Fingerprint Linear Estimation Routine to identify topology changes in power networks using readings from sparsely deployed phasor measurement units (PMUs). When a power line, load, or generator trips in a network, or when a substation is reconfigured, the event leaves a unique "voltage fingerprint" of bus voltage changes that we can identify using only the portion of the network directly observed by the PMUs. The naive brute-force approach to identify a failed line from such voltage fingerprints, though simple and accurate, is slow. We derive an approximate algorithm based on a local linearization and a novel filtering approach that is faster and only slightly less accurate. We present experimental results by using the IEEE 57-bus, IEEE 118-bus, and Polish 1999-2000 winter peak networks.**

Index Terms—**Approximation, filtering, linearization, phasor measurement units, topology changes, voltage fingerprint.**

I. Introduction

A. Motivation

DETECTION of topology changes is important for network monitoring, and is a key part of the power grid state estimation pipeline, either as a pre-processing step or as an integrated part of a generalized state estimator. If a topology error processing module fails to detect an error in the model topology, poor and even dangerous control actions may result [1], [2], as unexpected topology changes, such as those due to failed lines, may stress the remaining lines and destabilize the network. Thus, it is important to identify topology changes quickly in order to take appropriate control actions.

Substations and transmission lines in transmission networks have sensors that directly report failures (or switch open/closed status). However, if a sensor malfunctions, then finding the topology change is again difficult. This can happen due to normal equipment malfunctions, or because a cyber-attacker wishes to mislead network operators. Although failure to correctly identify a topology error is less common in a transmission network, the stakes are higher: state estimation based on incorrect topology assumptions can lead to incorrect estimates, causing operators to overlook system instability, and in the worst case, leading to avoidable blackouts. Thus, it is important to have multiple ways to monitor topology.

B. Prior Work

SCADA-based state estimation and topology detection methods have co-evolved since at least the late 1970s [3]; see [4] for an overview of the state of the art as of 2000. Because SCADA sensors report power flows rather than directly reporting current and voltage phasors, state estimators traditionally must solve the nonlinear power flow equations. Moreover, SCADA sensors report at most every few seconds, and are not time-synchronized. Consequently, state (and topology) estimates may be computed minutes apart. Inter-area monitoring information arrives even more slowly; the system data exchange (SDX) model of the North American Electric Reliability Corporation (NERC) provides inter-area topology information only on an hourly basis [5].

In the twenty-first century, researchers have increasingly proposed monitoring based on phasor measurement units (PMUs), GPS-synchronized sensors that report voltage and current phasors at rates of 10–30 times per second [6]–[8]. PMU-based methods yield state estimates [9]–[11], information about oscillations [12]–[15], and indicators of faults or contigencies [16], [17] without SCADA data and with little or no reference to a system model during regular operation. These "model-free" methods are attractive because power system models are often not wholly correct.

Beside the challenges inherent in collecting and processing sensor data at very high bandwidths, there are two other major challenges to PMU-based monitoring. First, current PMU deployments are sparse; and, despite work on on placing PMUs to maximize observability [18]–[20], not every bus will be measured directly. The second challenge involves data quality: the IEEE specification specifies tight phase and magnitude error tolerances for PMUs [21], but deployed PMUs sometimes have errors greater than those nominally allowed by the standard [22]–[25], whether due to poor GPS synchronization (which may cause persistent phase errors), deficiencies in the signal processing algorithms (which may cause oscillations in the PMU output), or other issues.

Power researchers have proposed a variety of *hybrid* state estimation methods (also called *dynamic* state estimators) that combine SCADA data and PMU data; see [26]–[35] and the

Manuscript received March 7, 2016; revised July 14, 2016 and November 29, 2016; accepted January 14, 2017. Date of publication January 31, 2017; date of current version October 18, 2017. This work was supported in part by the Advanced Research Projects Agency-Energy (ARPA-E), U.S. Department of Energy, under Award DE-AR0000230, in part by an agency of the United States Government, and in part by the Government support under and awarded by DoD, Air Force Office of Scientific Research, National Defense Science and Engineering Graduate under Fellowship 32 CFR 168a. Paper no. TPWRS-00366-2016.

The authors are with the Department of Computer Science, Cornell University, Ithaca, NY 14850 USA (e-mail: cponce@cs.cornell.edu; bindel@cs.cornell.edu).

Color versions of one or more of the figures in this paper are available online at http://ieeexplore.ieee.org.

Digital Object Identifier 10.1109/TPWRS.2017.2662002

many references therein. Most of these methods use extended Kalman filters or some related data fusion mechanism to deal with sensor noise. Robust regression is also used in several hybrid state estimators [11], [26], [28], [33] to detect and handle gross errors, whether they come from PMUs or from SCADA sensors. The methods in this paper use differences between PMU reports, so are insensitive to absolute phase errors; and we filter the signal to reduce sensitivity to deficiencies in signal processing algorithms and to ambient oscillations. But we also use robust regression to defend against other types of errors.

Loss functions such as least absolute variation (LAV) or Huber loss [11], [36] provide robustness to inconsistent outlier equations caused by bad data or by errors in the model topology. But the shape of residuals associated with the outlier equations reflects topology errors, and a quarter century of work on SCADA topology estimators exploits this [37]–[42]. A few very recent works similarly incorporate fault detection as a part of a hybrid state estimator [26], [31]. Other proposed techniques for PMU-based fault detection and identification run independently of state estimation, or as a pre- or post-processor. Some are based on empirical signatures learned from PMU measurements with no model [17] or from simulated fault dynamics [16]. Other methods use a model-based approach to derive signatures for the failures. The method closest to our work is [43], [44] for diagnosing failure of one or two lines; related methods use lasso and similar approaches to find a set of tripped lines [45]–[48]. Other methods to detect line trips include [49]–[51]; but we are aware of only one proposed PMU-based method for monitoring substations [52]. Our work extends these prior approaches by using PMU signals to identify not only line trips, but also load trips, generator trips, and substation reconfigurations.

As with many SCADA topology estimation techniques, we model possible substation reconfigurations using a breaker-level model [36], [53]–[56]. While some methods use expanded bus-section models only in regions where a substation reconfiguration is suspected [57], we use a fixed breaker-level model and an extended system with a minimal set of multipliers corresponding to the edges in trees associated with each connected set of bus sections [58], [59].

C. Our Work

We present here an efficient method to identify topology changes in networks with a (possibly small) number of PMUs. We assume that a complete state estimate is obtained shortly before a topology change, e.g. through conventional SCADA measurements, and we use discrepancies between this state estimate and PMU measurements to identify failures. Our method does not require complete observability from PMU data; it performs well even when there are few PMUs in the network, though having more PMUs does improve the accuracy. Though our approach is similar in spirit to [43], this paper makes three key novel contributions:

1) We treat not only line outages, but also load trips, generator trips, and substation reconfigurations. This is not new for standard topology estimators, but to our knowledge it is new for PMU-based methods.
2) We describe a novel subspace-based filtering method to rule out candidate topology changes at low cost.
3) We take advantage of existing state estimation procedures by linearizing the full AC power flow about a previously estimated state. This increases accuracy compared to the DC approximation used in prior work.

II. Problem Formulation and Fingerprints

Let $y_{ik} = g_{ik} + \jmath b_{ik}$ denote the elements of the admittance matrix $Y \in \mathbb{C}^{n\times n}$ in a bus-branch network model; let P_ℓ and Q_ℓ denote the real and reactive power injections at bus ℓ; and let $v_\ell = |v_\ell| \exp(\jmath\theta_\ell)$ denote the voltage phasor at bus ℓ. These quantities are related by the power flow equations

$$H(v;Y) - s = 0 \tag{1}$$

where

$$\begin{bmatrix} H_\ell \\ H_{n+\ell} \end{bmatrix} = \sum_{h=1}^{n} |v_\ell||v_h| \begin{bmatrix} g_{\ell h} & b_{\ell h} \\ -b_{\ell h} & g_{\ell h} \end{bmatrix} \begin{bmatrix} \cos(\theta_{\ell h}) \\ \sin(\theta_{\ell h}) \end{bmatrix}, \tag{2}$$

with $\theta_{\ell h} = \theta_\ell - \theta_h$ and

$$s = \begin{bmatrix} P_1 & \cdots & P_n & Q_1 & \cdots & Q_n \end{bmatrix}^T. \tag{3}$$

We note that H is quadratic in v, but linear Y.

In a breaker-level model, we use a similar system in which variables are associated with bus sections, and H represents the power flows when all breakers are open. We then write the power flow equations as

$$\begin{aligned} H(v;Y) + C\lambda - s &= 0 \\ C^T v &= b, \end{aligned} \tag{4}$$

where the constraint equations $C^T v = b$ have the form

$$c_k^T v = (e_i - e_j)^T v = v_i - v_j = b_k = 0,$$

i.e. voltage variable j for a “slave” bus section is constrained to be the same as voltage variable i for a “master” bus section. In addition, we include constraints of the form

$$c_k^T v = e_i^T v = b_k$$

to assign a voltage magnitude at a PV bus or the phase angle at a slack bus. We could trivially eliminate these constraints, but keep them explicit for notational convenience.

Our goal is to use the power flow equations to diagnose topology changes such as single line failures, substation reconfigurations, or load or generator trips. We assume the network remains stable and the state shifts from one quasi-steady state to another. In practice, of course, there may be oscillations, whether due to ringdown after a topology change or ambient forcing; hence we recommend applying a low-pass filter to extract the mean behavior at each quasi-steady state. Under a topology update, the voltage vector shifts from v to $\hat{v} = v + \Delta v$. We assume m voltage phasor components, indicated by the rows of $E \in \{0,1\}^{m\times n}$, are directly observed by PMUs, with appropriate filtering. Assuming the loads and generation vary slowly, modulo high-frequency fluctuations removed by the low-pass filter, we can predict what $E\Delta v$ should be for each possible contingency. That is, we can match the observed voltage changes $E\Delta v$ to a list of *voltage fingerprints* to identify simple topology changes. We note that the same approach used to produce fingerprints for load and generator trips can also be used to identify significant changes in load or generation at a single source.

Multiple contingencies can have the same or practically indistinguishable fingerprints. For example, one of two parallel lines with equal admittance may fail, or two lines that are distant from all PMUs but near each other may yield similar fingerprints. But even when a contingency is not identifiable, our method still produces valuable information. When multiple lines have the same effect on the network, our technique can be used to identify a small set of potential lines or breakers to inspect more closely.

III. Approximate Fingerprints

To compute the exact fingerprint for a contingency, we require a nonlinear power flow solve. In a large network with many possible contingencies, this computation becomes expensive. We approximate the changing voltage in each contingency by linearizing the AC power flow equations about the pre-contingency state. As in methods based on the DC approximation, we use the structure of changes to the linearized system to compute voltage change fingerprints for each contingency with a few linear solves. By using information about the current state, we observe better diagnostic accuracy with our AC linearization than with the DC approximation.

We consider three different types of contingencies: bus merging or bus splitting due to substation reconfiguration, and line failure. In each case, we assume the pre-contingency state is $x = (v, \lambda)$ satisfying (4). We denote the post-contingency state by primed variables $x' = (v', \lambda')$; we assume in general that the power injections s are the same before and after the contingency. The exact shift in state is $\Delta x' = x' - x$, and our approximate fingerprints are based from the approximation $\delta x' \approx \Delta x$ to the shift in state. The computation of $\delta x'$ for each contingency involves the pre-contingency Jacobian matrix

$$A = \begin{bmatrix} \frac{\partial H}{\partial v}(v;Y) & C \\ C^T & 0 \end{bmatrix}.$$

We assume a factorization of A is available, perhaps from a prior state estimate.

A. Bus Merging Fingerprints

In the case of two bus sections becoming electrically tied due to a breaker closing, we augment C by two additional constraints C' to tie together the voltage magnitudes and phase angles of the previously-separate bus sections. That is, the post-contingency state satisfies the augmented system

$$\begin{aligned} H(v';Y) + C\lambda' + C'\gamma - s &= 0 \\ C^T v' &= b \\ C'^T v' &= 0. \end{aligned} \tag{5}$$

We linearize (5) about the original state x (with $\gamma = 0$); because the first two equations are satisfied at this state, we have the approximate system

$$\begin{bmatrix} A & U \\ U^T & 0 \end{bmatrix} \begin{bmatrix} \delta x' \\ \gamma \end{bmatrix} = - \begin{bmatrix} 0 \\ C'^T v \end{bmatrix}, \quad U = \begin{bmatrix} C' \\ 0 \end{bmatrix} \tag{6}$$

We then solve the system by block elimination to obtain

$$\gamma = (U^T A^{-1} U)^{-1} (C'^T v) \tag{7}$$

$$\delta x' = -A^{-1} U \gamma \tag{8}$$

The formulas (7)–(8) only require two significant linear solves (to evaluate $A^{-1}U$), some dot products, and a 2×2 solve.

B. Bus Splitting Fingerprints

When a bus splits after a breaker opens, the post-contingency state satisfies the augmented system

$$\begin{aligned} H(v';Y) + C\lambda' - s &= 0 \\ C^T v' + F\gamma &= b \\ F^T \lambda' &= 0. \end{aligned} \tag{9}$$

The slack variables γ let the voltage phasor for a "breakaway" group of previously-slaved sections differ from a phasor at the former master section. The two columns of $F \in \{0,1\}^{n \times 2}$ indicate rows of C^T that constrain the breakaway voltage magnitudes and the phase angles, respectively. The third equation says no power flows across the open breaker.

We linearize (9) about the original state x (with $\gamma = 0$); because the first two equations are satisfied at this state, we have the approximate system

$$\begin{bmatrix} A & U \\ U^T & 0 \end{bmatrix} \begin{bmatrix} \delta x' \\ \gamma \end{bmatrix} = - \begin{bmatrix} 0 \\ F^T \lambda \end{bmatrix}, \quad U = \begin{bmatrix} 0 \\ F \end{bmatrix}. \tag{10}$$

The bordered systems (10) has the same form as (6); and, as before, block Gaussian elimination requires only two solves with A, some dot products, and a 2×2 system solve.

C. Load/Generator Trip Fingerprints

When a load or generator trips offline, that bus becomes a zero-injection PQ nodes. In the case of a PQ load tripping offline, the network itself does not change, so we do not need to augment the matrix A as is done in Equations (6) and (10), but we compute the approximate fingerprint with just A. Rather, it is the power injection vector s that changes.

In the case of a generator at a PV bus tripping offline, we need to convert that bus into a PQ bus with zero power injection. We write the augmented system

$$\begin{aligned} H(v';Y) + C\lambda' - s' &= 0 \\ C^T v' + f\gamma &= b \\ f^T \lambda' &= 0. \end{aligned} \tag{11}$$

The slack variable γ lets the voltage magnitude of the bus of interest shift. The vector f is an indicator vector such that the third equation constrains the reactive power injection slack variable to zero. Note that s has also been changed to s' to represent the real power injection shifting to zero.

The resulting system is

$$\begin{bmatrix} A & u \\ u^T & 0 \end{bmatrix} \begin{bmatrix} \delta x' \\ \gamma \end{bmatrix} = -\begin{bmatrix} 0 \\ f^T \lambda \end{bmatrix}, \quad u = \begin{bmatrix} 0 \\ f \end{bmatrix}. \tag{12}$$

The bordered system (12) has the same form as (10) and (6). In this case, only one solve with A is required.

D. Line Failure Fingerprints

In principle, line failures can be handled in the same way as substation reconfigurations that lead to bus splitting: explicitly represent two nodes on a line that are normally connected (physically corresponding to two sides of a breaker) with a multiplier that forces them to be equal, and compute the fingerprint by an extended system that negates the effect of that multiplier. In practice, we may prefer to avoid the extra variables in this model. The following formulation requires no explicit extra variables in the base model, and can be used with either a breaker-level model or a bus-branch model with no breakers (i.e. C an empty matrix).

For line failures, the admittance changes to $Y' = Y + \Delta Y'$ where $\Delta Y'$ is a rank-one update. The post-contingency state satisfies the system

$$\begin{aligned} H(v'; Y') + C\lambda' - s &= 0 \\ C^T v' &= b, \end{aligned}$$

and linearization about x gives

$$\begin{bmatrix} \frac{\partial H}{\partial v}(v; Y') & C \\ C^T & 0 \end{bmatrix} \begin{bmatrix} \delta v' \\ \delta \lambda' \end{bmatrix} = -\begin{bmatrix} H(v; \Delta Y') \\ 0 \end{bmatrix} \tag{13}$$

where $H(v; \Delta Y') = H(v; Y') - H(v; Y)$. As we show momentarily,

$$\frac{\partial H}{\partial v}(v; Y') - \frac{\partial H}{\partial v}(v; Y) = \frac{\partial H}{\partial v}(v; \Delta Y') = U^0 (V^0)^T.$$

where U^0 and V^0 each have three columns. That is, the matrix in the system (13) is a rank-three update to A. We can solve such a system by the Sherman-Morrison-Woodbury update formula, also widely known as the Inverse Matrix Modification Lemma [60], [61]. We use the equivalent extended system

$$\begin{bmatrix} A & U \\ V^T & -I \end{bmatrix} \begin{bmatrix} \delta x' \\ \gamma \end{bmatrix} = -\begin{bmatrix} r \\ 0 \end{bmatrix}, \tag{14}$$

where

$$U = \begin{bmatrix} U^0 \\ 0 \end{bmatrix}, \quad V = \begin{bmatrix} V^0 \\ 0 \end{bmatrix}, \quad r = \begin{bmatrix} H(v; \Delta Y') \\ 0 \end{bmatrix}.$$

We again solve by block elimination:

$$\gamma = (I + V^T A^{-1} U)^{-1} (V^T r) \tag{15}$$

$$\delta x' = -A^{-1}(r + U\gamma). \tag{16}$$

The work to evaluate (15)–(16) is three linear solves (for $A^{-1}U$), some dot products, and a small 3×3 solve. We will show momentarily how to avoid the solve involving r.

We now show that the Jacobian matrix changes by a rank-3 update. For a failed line between nodes i and k, the vector $H(v, \Delta Y')$ has only four nonzero entries:

$$\begin{aligned} \check{P}_i &\equiv H_i = \check{P}_{ik} + g'_{ii}|v_i|^2 \\ \check{Q}_i &\equiv H_{i+n} = \check{Q}_{ik} - b'_{ii}|v_i|^2 \\ \check{P}_k &\equiv H_k = \check{P}_{ki} + g'_{kk}|v_k|^2 \\ \check{Q}_k &\equiv H_{k+n} = \check{Q}_{ki} - b'_{kk}|v_k|^2, \end{aligned}$$

where

$$\begin{bmatrix} \check{P}_{ik} \\ \check{Q}_{ik} \end{bmatrix} \equiv |v_i||v_k| \begin{bmatrix} g'_{ik} & b'_{ik} \\ -b'_{ik} & g'_{ik} \end{bmatrix} \begin{bmatrix} \cos(\theta_{ik}) \\ \sin(\theta_{ik}) \end{bmatrix},$$

and $\check{P}_{ki}, \check{Q}_{ki}$ are defined similarly. Let

$$D_{ik} \equiv \frac{\partial(\check{P}_i, \check{P}_k, \check{Q}_i, \check{Q}_k)}{\partial(\theta_i, \theta_k, |v|_i, |v|_k)} \in \mathbb{R}^{4\times 4};$$

by the chain rule, we can write $D_{ik} = U_{ik} V_{ik}^T$ where

$$U_{ik} \equiv \frac{\partial(\check{P}_i, \check{P}_k, \check{Q}_i, \check{Q}_k)}{\partial(\theta_{ik}, \log|v|_i, \log|v|_k)} \in \mathbb{R}^{4\times 3}$$

$$V_{ik}^T \equiv \frac{\partial(\theta_{ik}, \log|v|_i, \log|v|_k)}{\partial(\theta_i, \theta_k, |v|_i, |v|_k)} \in \mathbb{R}^{3\times 4}.$$

More concretely, we have

$$U_{ik} = \begin{bmatrix} -\check{Q}_i - b'_{ii}|v_i|^2 & \check{P}_i + g'_{ii}|v_i|^2 & \check{P}_i - g'_{ii}|v_i|^2 \\ \check{Q}_k + b'_{kk}|v_k|^2 & \check{P}_k - g'_{kk}|v_k|^2 & \check{P}_k + g'_{kk}|v_k|^2 \\ \check{P}_i - g'_{ii}|v_i|^2 & \check{Q}_i - b'_{ii}|v_i|^2 & \check{Q}_i + b'_{ii}|v_i|^2 \\ -\check{P}_k + g'_{kk}|v_k|^2 & \check{Q}_k + b'_{kk}|v_k|^2 & \check{Q}_k - b'_{kk}|v_k|^2 \end{bmatrix}$$

$$V_{ik}^T = \begin{bmatrix} 1 & -1 & 0 & 0 \\ 0 & 0 & |v_i|^{-1} & 0 \\ 0 & 0 & 0 & |v_k|^{-1} \end{bmatrix}.$$

Because $H(v, \Delta Y')$ does not depend on any voltage phasors other than those at nodes i and j, we may write

$$\frac{\partial H(v; \Delta Y')}{\partial v} = E_{ik} D_{ik} E_{ik}^T = U^0 (V^0)^T \tag{17}$$

where

$$E_{ik} = \begin{bmatrix} e_i & e_k & & \\ & & e_i & e_k \end{bmatrix} \in \mathbb{R}^{2n\times 4}. \tag{18}$$

and

$$U^0 = E_{ik} U_{ik}, \quad V^0 = E_{ik} V_{ik}. \tag{19}$$

Moreover, we note that

$$H(v, \Delta Y') = E_{ik} \begin{bmatrix} \check{P}_i \\ \check{P}_k \\ \check{Q}_i \\ \check{Q}_k \end{bmatrix} = U^0 z, \quad z = \begin{bmatrix} 0 \\ 1/2 \\ 1/2 \end{bmatrix},$$

so that we may rewrite (16) as

$$\delta x' = -A^{-1} U (z + \gamma). \tag{20}$$

Algorithm 1: FLiER.

Compute and store $\bar{E}A^{-1}$.
For each contingency i, compute τ_i via (23).
Order the contingencies in ascending order by τ.
for $\ell = 2, 3, \ldots$ **do**
  Compute fingerprint score t_ℓ
  Break if $t_\ell < \tau_{\ell+1}$
end for
Return contingencies with computed t_ℓ

IV. Filtering

In Section III we discussed how to approximate voltage shifts $\delta v'$ associated with several types of contingencies. This approach to predicting voltage changes costs less than a nonlinear power flow solve, but may still be costly for a large network with many contingencies to check. In the current section we show how to rule out contingencies without any solves by computing a cheap lower bound on the discrepancy between the observed voltage changes and the predicted voltage changes under the contingencies.

For each contingency, we define the *fingerprint score*

$$t = \|E\Delta v - E\delta v'\| \tag{21}$$

where Δv is the observed voltage shift and $\delta v'$ is the voltage shift predicted for the contingency. For the contingencies we have described, $E\delta v'$ has the form

$$E\delta v' = \bar{E}A^{-1}U\gamma \tag{22}$$

where $\bar{E} = \begin{bmatrix} E & 0 \end{bmatrix}$ simply ignores the multiplier variables λ, and γ is some short vector of slack variables. The expression $\bar{E}A^{-1}$ does not depend on the contingency, and can be precomputed at the cost of m linear solves (one per observed phasor component). After this computation, the main cost in evaluating (22) is the computation of γ, which involves a contingency-dependent linear system with A as an intermediate step. However, we do not need γ for the *filter score*

$$\tau = \min_{\mu} \|E\Delta v - \bar{E}A^{-1}U\mu\| \leq t. \tag{23}$$

In the Euclidean norm, τ is simply the size of the residual in a least squares fit of $E\Delta v$ to the columns of $\bar{E}A^{-1}U$, which can be computed quickly due to the sparsity of U. If U is the augmentation matrix associated with contingency i, we refer to $\bar{E}A^{-1}U$ as its *filtering subspace*.

Filter score computations are cheap; and if the filter score τ_i for contingency i exceeds the fingerprint score t_k for contingency k, then we know

$$t_k < \tau_i \leq t_i,$$

without ever computing t_i. Exploiting this fact leads to the FLiER method (Algorithm 1).[1]

We note that PQ load trips require no filtering, as they involve no change to the system matrix.

[1]Example Python code of this algorithm can be found at https://github.com/cponce512/FLiER_Test_Suite.

Filter score computations are embarrassingly parallel and can be spread across processors. Nonetheless, for huge networks with many PMUs and many contingencies, the filter computations might be deemed too expensive for very rapid diagnosis (e.g. in less than a second). However, the concept of a filter subspace can be adapted to these cases. First, one can define a *coarse* filtering subspaces that is the sum of the filtering subspaces for a set of contingencies. For example, one might define a coarse filtering subspace associated with all possible breaker reconfigurations inside a substation. The coarse subspace filter score provides a lower bound on the filter scores (and hence the fingerprint scores) for all contingencies in the set. Hence, it may not even be necessary to compute individual filter scores for all contingencies considered. Second, one can work with a *projected* filtering subspace $W^T(EA^{-1}U)$ where W is a matrix with orthonormal columns. The distance from a projected measurement vector to the projected filtering subspace again gives a lower bound on the full filter score. In addition to reducing the cost of filter score computations, projections can also be used to eliminate faulty or missing PMU measurements from consideration.

V. Experiments

Our standard experimental setup is as follows. For each possible topology change, we compute and pass to FLiER both the full pre-contingency state and the subset of the post-contingency state that would be observed by the PMUs. We test both with no noise and with independent random Gaussian noise with standard deviation $1.7 \cdot 10^{-3}$ (≈0.1 degrees for phase angles) added to both the initial state estimate and the PMU readings. In [43], 0.1 degrees of Gaussian random noise was applied to phase angles, then smoothed by passing a simulated time-domain signal through a low pass filter; we apply the noise without filtering, so the effect is more drastic.

One of the possibilities FLiER checks is that there has been no change; in this case, we use the norm of the fingerprint as both the fingerprint score and the filter score. By including this possibility among those checked, FLiER acts simultaneously as a method for topology change detection and identification.

We run tests on the IEEE 57 bus and 118 bus networks, with three different PMU arrangements on each:

1) *Single:* Only one PMU is placed in the network, at a low-degree node (bus 35 in the 57-bus network and 65 in the 118-bus network, providing a total of 3 and 5 bus voltage readings, respectively). This represents a near-worst-case deployment for our method.
2) *Sparse:* A few PMUs are placed about the network (on buses 4, 13, and 34 in the 57-bus network and on buses 5, 17, 37, 66, 80, and 100 in the 118-bus network, providing a total of 15 and 40 bus voltage readings, respectively). We consider this a realistic scenario in which sparsely-deployed PMUs do not offer full network observability.
3) *All:* PMUs are placed on all buses. Any error is due purely to the linear approximation.

We did not test changes that cause convergence failure in our power flow solver. We assume such contingencies result in collapse without some control action.

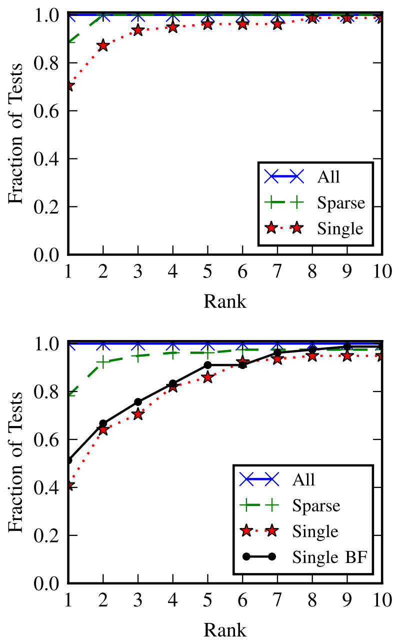

Fig. 1. Cumulative distribution function showing the fraction of line failures where FLiER assigned the correct line at most a given rank (up to 10). Top: Noise-free case. Bottom: Entries with Gaussian noise with $\sigma = 0.0017$. "Single BF" is the result from using a brute-force approach with a single PMU and represents the signal-to-noise ratio in that PMU's information.

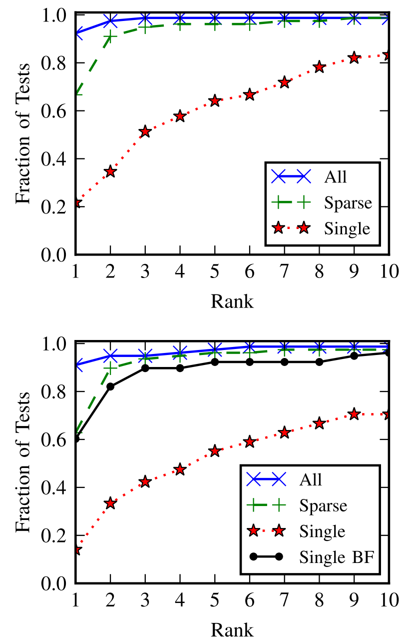

Fig. 2. CDF of line failures where the DC approximation of [43] assigned the correct line at most a given rank (up to 10). Top: Noise-free case. Bottom: Entries with Gaussian noise with $\sigma = 0.0017$. "Single BF" is the result from using a brute-force approach with a single PMU and represents the signal-to-noise ratio in that PMU's information.

TABLE I
IEEE 57-Bus Network Accuracy Comparison for 78 Line Failure Contingencies. We Report Counts of Line Failures Correctly Identified and Those Scored in the Top Three (in Parentheses)

PMUs	Single	Sparse	All
FLiER	55(73)	68(77)	78(78)
FLiER+noise	40(65)	66(78)	78(78)
DC Approx	17(40)	52(74)	72(77)
DC Approx+noise	5(22)	49(64)	66(68)

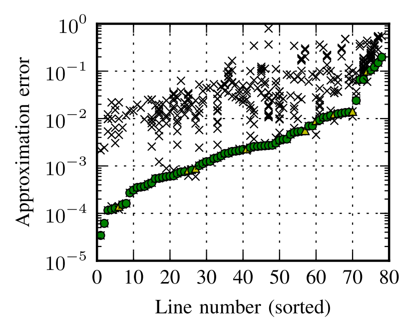

Fig. 3. Test of our algorithm on the IEEE 57-bus network with the sparse PMU deployment. Each column represents one test. Black crosses are fingerprint scores for incorrect lines. Green dots and yellow triangles indicate the scores of the correct line in the case of correct diagnosis or diagnosis in the top three, respectively.

A. Accuracy

1) Line Failures: Fig. 1 shows the accuracy of FLiER in identifying line failures in the IEEE 57-bus test network. For each PMU deployment, we show the cumulative distribution function of ranks, i.e. the ranks of each simulated contingency in the ordered list produced by FLiER. We show further results in Table I. With PMUs everywhere, the correct answer was chosen in all 78 of 78 cases, even in the presence of noise. The case with three PMUs is also quite robust to noise. In the test with a single unfavorably-placed PMU, FLiER typically ranks the correct line among the top three in the absence of noise; with noise, the accuracy degrades, though not completely.

In Fig. 2, we repeat the experiment of Fig. 1, but with the DC approximation used in [43] rather than the AC linearization used in FLiER. We also present comparisons in Table I. With PMUs everywhere, there is little difference in accuracy. With fewer PMUs, FLiER is more accurate. In the sparse case, the DC approximation without noise behaves similarly to FLiER with noise, while in the single PMU deployment the DC results without noise are much worse than those from FLiER even with noise.

Fig. 3 shows the raw scores computed by FLiER with three PMUs. In this plot, each column represents the fingerprint scores computed for one line failure scenario. The black crosses represent the scores of lines that get past the filter, while the green circles and yellow triangles represent the scores for the correct answer. If there is a green circle, then our algorithm correctly identified the actual line that failed. If there is a yellow triangle, the correct line was not chosen but was among the top three lines selected by the algorithm.

In Fig. 4, we show one case that FLiER misidentifies. PMUs are deployed on buses marked with blue squares, and lines are

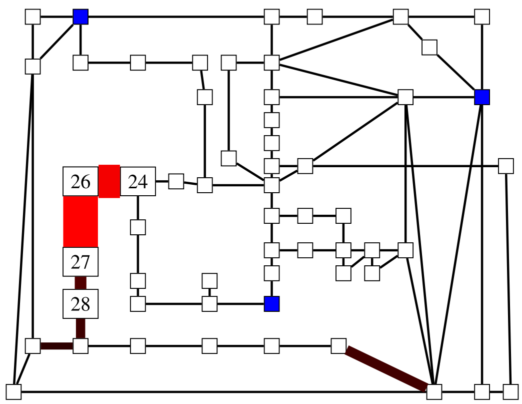

Fig. 4. Line (24, 26) is the line removed in this test. Lines are colored and thickened according to $\sqrt{t_{ik}^{-1}}$. Line (26, 27) was chosen by the algorithm.

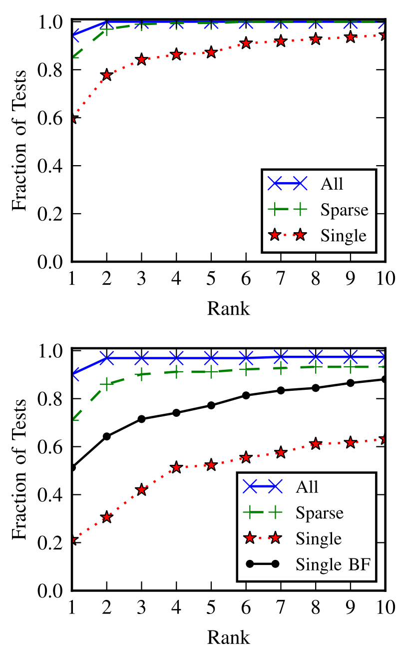

Fig. 5. Rank CDF for substation reconfigurations without noise (top) and with noise (bottom). "Single BF" is the result from using a brute-force approach with a single PMU and represents the signal-to-noise ratio in that PMU's information.

colored and thickened according to the FLiER score. The best-scoring line is adjacent to the line that failed.

2) Substation Reconfigurations: Next, we show the accuracy of FLiER as it applies to substation reconfigurations. For these tests, we suppose that every bus in the IEEE 57-bus test network is a ring substation with each bus section on the ring possessing either load, generation, or a branch. We then suppose a substation splits when two of its circuit breakers open. We do not consider cases that isolate a node with a nonzero power injection. Line failures are a subset of this scenario: if the breakers on either side of a section with a branch open, that section becomes a zero-injection leaf bus, which disappears in the quasi-static setting.

Fig. 5 shows the accuracy of FLiER on substation reconfigurations with and without noise. With three PMUs and no noise,

TABLE II
ACCURACY OF FLiER WITH 100 RANDOMLY-PLACED PMUS ON THE POLISH NETWORK. RESULTS ARE OUT OF 6283 TESTS

	Contingency	Substation of Contingency
Correct %	75.2	85.4
Top 3%	95.4	96.5

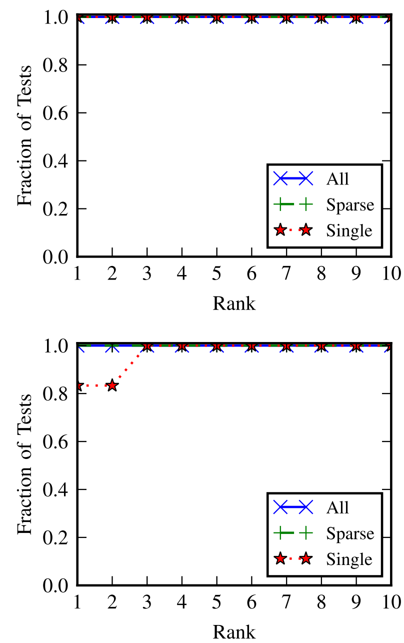

Fig. 6. Rank CDF for generator trips without noise (top) and with noise (bottom).

FLiER is right in 164 of 193 possibilities, and ranks the correct answer among the top three scores in 160 cases. With PMUs everywhere, FLiER is right 181 times, but gets the answer in the top three every single time. With few PMUs, FLiER is more susceptible to noise when diagnosing substation reconfigurations. This is expected, as there are significantly more possibilities to choose from in this case. Also, FLiER sometimes filters out the correct answer in the presence of noise. One possible remedy for this would be to be more lenient with filtering, only throwing a possibility away if τ_ℓ is greater than the kth smallest t_ℓ, for example.

Finally, we demonstrate the effectiveness of using FLiER for substation reconfigurations on a large-scale network by running FLiER on the 400, 220, and 100 kV subset of the Polish network during peak conditions of the 1999–2000 winter, taken from [62]. This is a larger network with 2,383 buses. We placed 100 PMUs randomly around the network, and tested every substation reconfiguration contingency. We summarize the results in Table II. We could likely further improve the accuracy with a thoughtful deployment of PMUs.

3) Including Load and Generator Trips: Here we include load and generator trips in our results. In Fig. 6, we show the results of testing for generator trips, in Fig. 7, we show the results

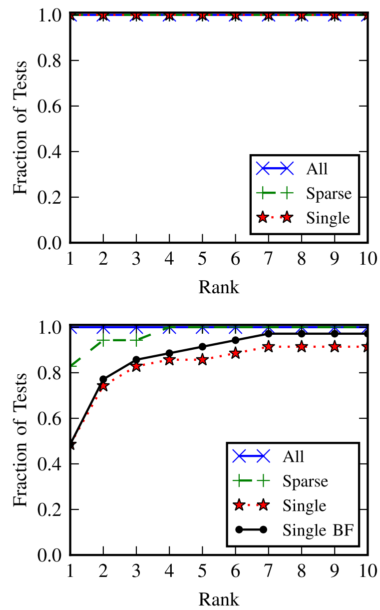

Fig. 7. Rank CDF for load trips without noise (top) and with noise (bottom). In the noisy case, we allow a filtering slack equal to one noise standard deviation, as otherwise the filter is too stringent. “Single BF” is the result from using a brute-force approach with a single PMU and represents the signal-to-noise ratio in that PMU’s information. We do not include zero-injection busses in this test.

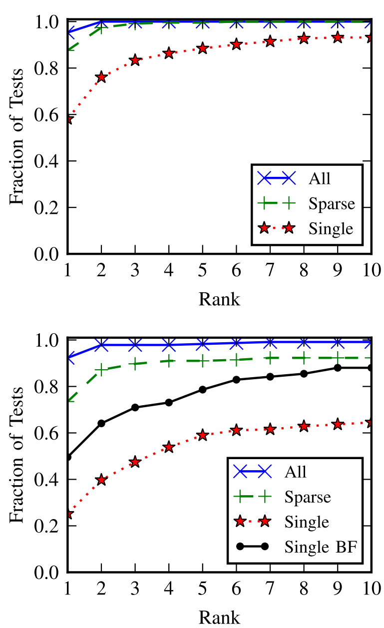

Fig. 8. Rank CDF for substation reconfigurations and load/generator trips without noise (top) and with noise (bottom). “Single BF” is the result from using a brute-force approach with a single PMU and represents the signal-to-noise ratio in that PMU’s information.

of testing for load trips, and in Fig. 8, we show the results of including load and generator trips in the set of contingencies to test and check for along with substation splits. All tests use the IEEE 57-bus network.

In the noisy case for Fig. 7, we allow some extra slack in the filtering procedure. In particular, rather than checking if $t_k < \tau_i$, we check if $t_k < \tau_i - \sigma$, where σ is the standard deviation of the included noise. We did this because the filtering method

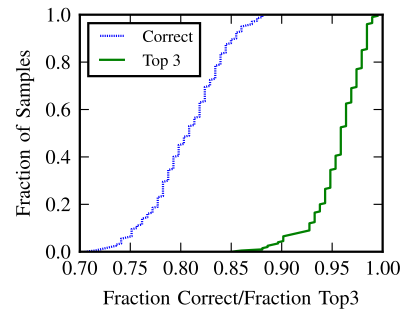

Fig. 9. CDF for fraction of substation reconfiguration contingencies that FLiER gets correct (blue) and in the top 3 (green) with random uniform placement of three PMUs. Noise is not included in this test.

sometimes filtered out the correct answer for load trips. In a real-world setting one would need to choose that slack value intelligently, but this test shows that slightly less-stringent filtering can improve the method in some cases.

4) PMU Placement: Here we demonstrate the robustness of FLiER to PMU placement. We tested this by sampling three busses from the IEEE 57-bus network uniformly at random, running FLiER for the substation reconfiguration case (as in Fig. 5) and recording the fraction of contingencies FLiER identified correctly, and the fraction of contingencies with the solution ranked in the top 3. We performed this test 200 times. We show cumulative distribution functions for the fraction correct and fraction in the top 3 in Fig. 9.

This figure shows that FLiER tends to be quite robust to PMU placement. In fact, the median fraction correct and median fraction in top 3 are only slightly below those for the noiseless test in Fig. 5, where we attempted to place the three PMUs favorably. Furthermore, the standard deviation for fraction correct is only 3.65%, while the standard deviation for fraction in top 3 is 2.67%.

5) Robustness to Bad Data: Here we demonstrate how one can easily modify FLiER for enhanced robustness to bad data and heavy-tailed noise. In Equations (21) and (23), we use the L2 loss function to measure the distance between an estimated fingerprint or subspace and the actual fingerprint. The L2 loss function, while simple and useful, is sensitive to outliers. A single large error component drastically increases the t or τ value, even if all other components have very small error. The result is using the L2 loss can make FLiER sensitive to bad data and heavy-tailed noise.

An alternative is to use a loss function that is robust to large outliers. One popular such loss function is the *Huber loss* [36]:

$$\|e\|_H^2 = \sum_{i=1}^{m} L_\delta(e_i) \tag{24}$$

$$L_\delta(e_i) = \begin{cases} \frac{1}{2}e_i^2 & |e_i| \le \delta \\ \delta\left(|e_i| - \frac{1}{2}\delta\right) & \text{otherwise} \end{cases} \tag{25}$$

This function behaves like the L2 loss for error components near zero, but for error components larger than δ, the loss grows linearly rather than quadratically. The result is a loss function that is robust to outliers in data.

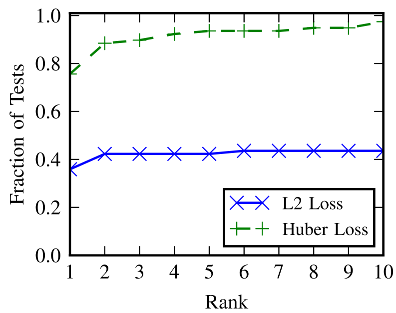

Fig. 10. CDF for line failures with a single PMU reading that systematically gives angle readings that are too large by 5 degrees, along with Gaussian random noise with standard deviation 0.0017. PMUs are at locations 4, 13, and 34. Huber scale parameter $\delta = 1.365 \cdot 0.0017$.

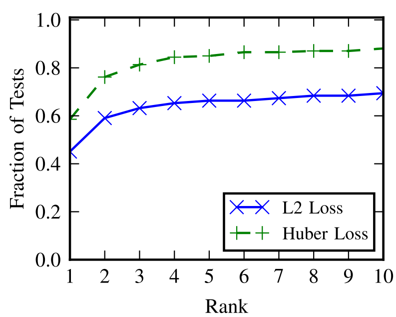

Fig. 11. CDF for substation reconfigurations with Cauchy noise with a scale parameter of 0.001.

In Figs. 10 and 11 we show the usefulness of the Huber loss in certain cases. In Fig. 10, we run FLiER on the line failures test (as in the noisy case of Fig. 1), but with the PMU reading from bus 4 given a large post-event bias, always returning an after-event angle reading that is 5 degrees too large. As shown in the figure, this single bad reading can cause major problems with FLiER accuracy using L2 loss. With Huber loss, however, that bad data is almost completely ignored, resulting in accuracy essentially identical to that of the noisy case in Fig. 1.

In Fig. 11, we show the utility of the Huber loss in the presence of heavy-tailed noise. Here we test substation reconfigurations with noise given by a Cauchy distribution with scale parameter 0.001. As shown in the figure, the use of the Huber loss significantly improves FLiER's performance under this type of noise.

It is unclear if either of these situations are likely to arise in practice. In the former case (with a bad PMU), it is likely that this bad data stream would be identified in an earlier state estimation stage and already removed from the fingerprint. In the latter case, the IEEE specification [21] requires that the PMU noise profile not have heavy tails, so systematic heavy-tailed noise is unlikely.

B. Filter Effectiveness and Speed

The cost of FLiER depends strongly on the effectiveness of the filtering procedure. In Fig. 12, we show how often the filter saves us from computing fingerprint scores in experiments on the IEEE 57-bus and 118-bus networks when checking for line failures. For each PMU deployment, we show the cumulative

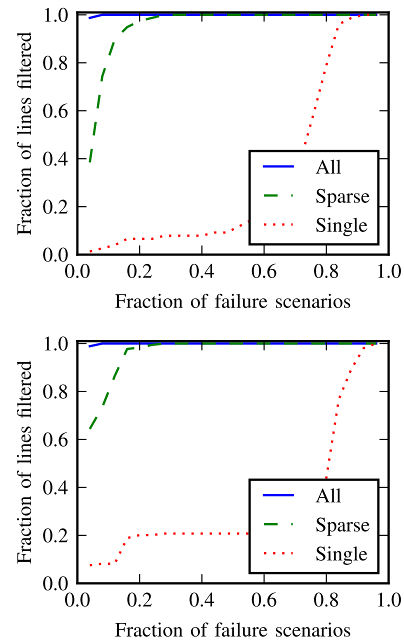

Fig. 12. Cumulative distribution function of fraction of lines for which t_{ik} need not be computed when a line in the IEEE 57-bus (top) or 118-bus (bottom) network fails uniformly at random.

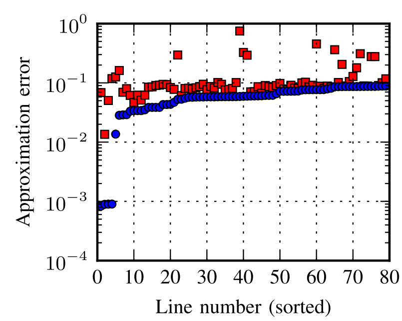

Fig. 13. Example of effective filtering in Algorithm 1. Each column represents a line checked. Blue dots are the lower bounds τ_{ik}, while red squares are true scores t_{ik}. Columns are sorted by τ_{ik}. In this case, t_{ik} only needs to be computed for eight lines.

distribution function of the fraction of lines for which fingerprint scores need not be computed for each line failure. The filter performs well even for the sparse PMU deployments; we show a typical case in Fig. 13.

Finally, we demonstrate the importance of the filter by running FLiER on the large Polish network [62] with 100 randomly placed PMUs. Table III shows FLiER run times with and without the filter on ten randomly selected branches. The code is unoptimized Python, so these timings do not indicate of how fast FLiER would run in a performance setting. However, they give a sense of the speedup one expects from filtering.

Note also that FLiER correctly identified the failed branch in 9 of 10 cases. In the one case in which it failed, on branch (2346, 2341), t_ℓ for the correct answer was $6.25 \cdot 10^{-5}$; this suggests the failure had a negligible impact on the network.

We also performed this timing test for a randomly selected set of substation reconfigurations, shown in Table IV. Again,

TABLE III
FLiER RUN TIMES FOR TEN LINE FAILURES WITH AND WITHOUT FILTERING. ABOUT 3000 CONTINGENCIES ARE CONSIDERED

Line	FLiER (s)	Solution rank	# t's computed	FLiER n.f. (s)
(1502, 917)	0.27	1	2	14.14
(1502, 1482)	0.27	1	2	15.30
(557, 556)	0.27	1	4	14.75
(2346, 2341)	2.95	14	502	14.40
(909, 1155)	0.26	1	2	14.32
(644, 629)	0.29	1	7	14.59
(591, 737)	0.29	1	6	17.27
(559, 542)	0.32	1	13	16.59
(378, 336)	0.28	1	6	16.16
(101, 94)	0.26	1	2	15.29

TABLE IV
FLiER RUN TIMES FOR TEN SUBSTATION RECONFIGURATIONS WITH AND WITHOUT FILTERING. NEARLY 7000 CONTINGENCIES ARE CONSIDERED

Bus /Split nodes	FLiER (s)	Sol. rank /Sol. bus rank	# t's computed	FLiER n.f. (s)
86/1,2,3	4.54	1/1	2	823.0
176/1,2	4.70	3/3	4	836.9
539/7	8.11	1/1	38	829.8
702/4,5	4.66	1/1	4	820.1
754/2,3,4,5	4.97	1/1	7	829.8
994/2,3,4,5	4.86	1/1	6	835.8
1131/2	5.22	1/1	9	850.3
1513/4,5,6	6.65	4/1	23	862.3
1663/1,2,3,4	7.83	1/1	35	928.1
2164/5	4.56	1/1	3	875.3

the results give a sense of the speedup one expects from filtering in the substation reconfiguration case.

VI. CONCLUSION AND FUTURE WORK

We have presented FLiER, a new algorithm to identify topology changes involving load and generator trips, line outages, and substation reconfigurations using a sparse deployment of PMUs. Our method uses a linearization of the power flow equations together with a novel subspace-based filtering approach to provide fast diagnosis. Unlike prior approaches based on DC approximation, our approach takes advantage of a state estimate obtained shortly before the topology changes, assuming that the network specifications remain unchanged or change in a known way as a result of the failure.

Several extensions remain open for future work. We hope to model noise sensitivity of our computations, so that we can provide approximate confidence intervals for fingerprint and filter scores; we also believe it possible to diagnose when the linear approximation will lead to incorrect diagnosis, and do more computation to deal just with those cases. In addition, we plan to extend our approach to other events, such as single-phase line failures or changes in line parameters due to overloading.

ACKNOWLEDGMENT

Neither the United States Government nor any agency thereof, nor any of their employees, makes any warranty, express or implied, or assumes any legal liability or responsibility for the accuracy, completeness, or usefulness of any information, apparatus, product, or process disclosed, or represents that its use would not infringe privately owned rights. Reference herein to any specific commercial product, process, or service by trade name, trademark, manufacturer, or otherwise does not necessarily constitute or imply its endorsement, recommendation, or favoring by the United States Government or any agency thereof. The views and opinions of authors expressed herein do not necessarily state or reflect those of the United States Government or any agency thereof.

REFERENCES

[1] A. Ashok and M. Govindarasu, "Cyber attacks on power system state estimation through topology errors," in *Proc. IEEE PES Meeting*, 2012, pp. 1–8.
[2] E. Caro, A. J. Conejo, and A. Abur, "Breaker status identification," *IEEE Trans. Power Syst.*, vol. 25, no. 2, pp. 694–702, May 2010.
[3] R. Lugtu, D. Hackett, K. Liu, and D. Might, "Power system state estimation: Detection of topological errors," *IEEE Trans. Power App. Syst.*, vol. PAS-99, no. 6, pp. 2406–2412, Nov. 1980.
[4] A. Monticelli, "Electric power system state estimation," *Proc. IEEE*, vol. 88, no. 2, pp. 262–282, Feb. 2000.
[5] U.S.-Canada Power System Outage Task Force, "Final report on the implementation of the task force recommendation," Sep. 2006. [Online]. Available: http://energy.gov/oe/downloads/ blackout-2003-blackout-final-implementation-report
[6] F. Aminifar, M. Fotuhi-Firuzabad, A. Safdarian, A. Davoudi, and M. Shahidehpour, "Synchrophasor measurement technology in power systems: Panorama and state-of-the-art," *IEEE Access*, vol. 2, no. 1, pp. 1607–1628, Jan. 2015.
[7] J. D. L. Ree, V. Centeno, J. S. Thorp, and A. G. Phadke, "Synchronized phasor measurement applications in power systems," *IEEE Trans. Smart Grid*, vol. 1, no. 1, pp. 20–27, Jun. 2010.
[8] A. G. Phadke and J. S. Thorp, *Synchronized Phasor Measurements and Their Applications*. New York, NY, USA: Springer, 2008.
[9] T. Yang, H. Sun, and A. Bose, "Transition to a two-level linear state estimator - part I: Architecture," *IEEE Trans. Power Syst.*, vol. 26, no. 1, pp. 46–53, Feb. 2011.
[10] T. Yang, H. Sun, and A. Bose, "Transition to a two-level linear state estimator - part II: Algorithm," *IEEE Trans. Power Syst.*, vol. 26, no. 1, pp. 54–62, Feb. 2011.
[11] M. Gö and A. Abur, "LAV based robust state estimation for systems measured by PMUs," *IEEE Trans. Smart Grid*, vol. 5, no. 4, pp. 1808–1814, Jul. 2014.
[12] N. Zhou, D. J. Trudnowski, J. W. Pierre, and W. A. Mittelstadt, "Electromechanical mode online estimation using regularized robust RLS methods," *IEEE Trans. Power Syst.*, vol. 23, no. 4, pp. 1670–1680, Nov. 2008.
[13] N. Zhou, J. W. Pierre, and D. Trudnowski, "A stepwise regression method for estimating dominant electromechanical modes," *IEEE Trans. Power Syst.*, vol. 27, no. 2, pp. 1051–1059, May 2012.
[14] L. Dosiek, J. W. Pierre, and J. Follum, "A recursive maximum likelihood estimator for the online estimation of electromechanical modes with error bounds," *IEEE Trans. Power Syst.*, vol. 28, no. 1, pp. 441–451, Feb. 2013.
[15] L. Dosiek, N. Zhou, J. W. Pierre, Z. Huang, and D. J. Trudnowski, "Mode shape estimation algorithms under ambient conditions: A comparative review," *IEEE Trans. Power Syst.*, vol. 28, no. 2, pp. 779–787, May 2013.
[16] T. Guo and J. V. Milanović, "Online identification of power system dynamic signature using PMU measurements and data mining," *IEEE Trans. Power Syst.*, vol. 31, no. 3, pp. 1760–1768, May 2016.
[17] L. Xie, Y. Chen, and P. R. Kumar, "Dimensionality reduction of synchrophasor data for early event detection: Linearized analysis," *IEEE Trans. Power Syst.*, vol. 29, no. 6, pp. 2784–2794, Nov. 2014.
[18] V. Madani *et al.*, "PMU placement considerations–A roadmap for optimal PMU placement," in *Proc. 2011 IEEE/PES Power Syst. Conf. Expo.*, Mar. 2011, pp. 1–7.
[19] N. M. Manousakis, G. N. Korres, and P. S. Georgilakis, "Taxonomy of PMU placement methodologies," *IEEE Trans. Power Syst.*, vol. 27, no. 2, pp. 1070–1077, May 2012.

[20] A. S. Deese, T. Nugent, and S. Coppi, "A comparative study of optimal PMU placement algorithms for cost minimization," in *Proc. 2014 IEEE PES General Meeting Conf. Expo.*, Jul. 2014, pp. 1–5.

[21] K. E. Martin *et al.*, "An overview of the IEEE Standard C37.118.2. – Synchrophasor data transfer for power systems," *IEEE Trans. Smart Grid*, vol. 5, no. 4, pp. 1980–1984, Jul. 2014.

[22] M. A. Donolo and V. A. Centeno, "A fast quality assessment algorithm for phasor measurements," *IEEE Trans. Power Del.*, vol. 20, no. 4, pp. 2407–2413, Oct. 2005.

[23] Z. Huang, J. F. Hauer, and K. E. Martin, "Evaluation of PMU dynamic performance in both lab environments and under field operating conditions," in *Proc. 2007 IEEE Power Eng. Soc. General Meeting*, Jun. 2007, pp. 1–6.

[24] D. Shi, D. J. Tylavsky, and N. Logic, "An adaptive method for detection and correction of errors in PMU measurements," *IEEE Trans. Smart Grid*, vol. 3, no. 4, pp. 1575–1583, Dec. 2012.

[25] Y. h. Tang, G. N. Stenbakken, and A. Goldstein, "Calibration of phasor measurement unit at NIST," *IEEE Trans. Instrum. Meas.*, vol. 62, no. 6, pp. 1417–1422, Jun. 2013.

[26] J. Zhao *et al.*, "Power system real-time monitoring by using PMU-based robust state estimation method," *IEEE Trans. Smart Grid*, vol. 7, no. 1, pp. 300–309, Jan. 2016.

[27] L. Hu, Z. Wang, I. Rahman, and X. Liu, "A constrained optimization approach to dynamic state estimation for power systems including PMU and missing measurements," *IEEE Trans. Control Syst. Technol.*, vol. 24, no. 2, pp. 703–710, Mar. 2016.

[28] G. Valverde, S. Chakrabarti, E. Kyriakides, and V. Terzija, "A constrained formulation for hybrid state estimation," *IEEE Trans. Power Syst.*, vol. 26, no. 3, pp. 1102–1109, Aug. 2011.

[29] E. Ghahremani and I. Kamwa, "Dynamic state estimation in power system by applying the extended Kalman filter with unknown inputs to phasor measurements," *IEEE Trans. Power Syst.*, vol. 26, no. 4, pp. 2556–2566, Nov. 2011.

[30] M. Glavic and T. V. Cutsem, "Reconstructing and tracking network state from a limited number of synchrophasor measurements," *IEEE Trans. Power Syst.*, vol. 28, no. 2, pp. 1921–1929, May 2013.

[31] A. S. Costa, A. Albuquerque, and D. Bez, "An estimation fusion method for including phasor measurements into power system real-time modeling," *IEEE Trans. Power Syst.*, vol. 28, no. 2, pp. 1910–1920, May 2013.

[32] P. Yang, Z. Tan, A. Wiesel, and A. Nehorai, "Power system PMUs with imperfect synchronization," *IEEE Trans. Power Syst.*, vol. 28, no. 4, pp. 4162–4172, Nov. 2013.

[33] M. Göl and A. Abur, "A hybrid state estimator for systems with limited number of PMUs," *IEEE Trans. Power Syst.*, vol. 30, no. 3, pp. 1511–1517, May 2015.

[34] M. Göl and A. Abur, "A fast decoupled state estimator for systems measured by PMUs," *IEEE Trans. Power Syst.*, vol. 30, no. 5, pp. 2766–2771, Sep. 2015.

[35] N. Kashyap, S. Werner, Y. F. Huang, and T. Riihonen, "Power system state estimation under incomplete PMU observability—A reduced-order approach," *IEEE J. Sel. Topics Signal Process.*, vol. 8, no. 6, pp. 1051–1062, Dec. 2014.

[36] L. Mili, G. Steeno, F. Dobraca, and D. French, "A robust estimation method for topology error identification," *IEEE Trans. Power Syst.*, vol. 14, no. 4, pp. 1469–1476, Nov. 1999.

[37] M. R. Irving and M. J. H. Sterling, "Substation data validation," *IEE Proc. C, Gener., Transm., Distrib.*, vol. 129, no. 3, pp. 119–122, May 1982.

[38] K. Clements and P. Davis, "Detection and identification of topology errors in electric power systems," *IEEE Trans. Power Syst.*, vol. 3, no. 4, pp. 1748–1753, Nov. 1988.

[39] F. F. Wu and W.-H. E. Liu, "Detection of topology errors by state estimation," *IEEE Trans. Power Syst.*, vol. 4, no. 1, pp. 176–183, Feb. 1989.

[40] I. Costa and J. Leao, "Identification of topology errors in power system state estimation," *IEEE Trans. Power Syst.*, vol. 8, no. 4, pp. 1531–1538, Nov. 1993.

[41] A. Abur, H. Kim, and M. Celik, "Identifying the unknown circuit breaker statuses in power networks," *IEEE Trans. Power Syst.*, vol. 10, no. 4, pp. 2029–2037, Nov. 1995.

[42] H. Singh and F. L. Alvarado, "Network topology determination using least absolute value state estimation," *IEEE Trans. Power Syst.*, vol. 10, no. 3, pp. 1159–1165, Aug. 1995.

[43] J. E. Tate and T. J. Overbye, "Line outage detection using phasor angle measurements," *IEEE Trans. Power Syst.*, vol. 23, no. 4, pp. 1644–1652, Nov. 2008.

[44] J. E. Tate and T. J. Overbye, "Double line outage detection using phasor angle measurements," in *Proc. IEEE PES Meeting*, 2009, pp. 1–5.

[45] H. Zhu and G. B. Giannakis, "Lassoing line outages in the smart power grid," in *Proc. IEEE SmartGridComm.*, 2011, pp. 570–575.

[46] H. Zhu and G. B. Giannakis, "Sparse overcomplete representations for efficient identification of power line outages," *IEEE Trans. Power Syst.*, vol. 27, no. 4, pp. 2215–2224, Nov. 2012.

[47] G. Feng and A. Abur, "Fault location using wide-area measurements and sparse estimation," *IEEE Trans. Power Syst.*, vol. 31, no. 4, pp. 2938–2945, Jul. 2016.

[48] J. Wu, J. Xiong, and Y. Shi, "Efficient location identification of multiple line outages with limited PMUs in smart grids," *IEEE Trans. Power Syst.*, vol. 30, no. 4, pp. 1659–1668, Jul. 2015.

[49] P. Bhui and N. Senroy, "Online identification of tripped line for transient stability assessment," *IEEE Trans. Power Syst.*, vol. 31, no. 3, pp. 2214–2224, May 2016.

[50] C. Chen, J. Wang, and H. Zhu, "Effects of phasor measurement uncertainty on power line outage detection," *IEEE J. Sel. Topics Signal Process.*, vol. 8, no. 6, pp. 1127–1139, Dec. 2014.

[51] S. Azizi and M. Sanaye-Pasand, "A straightforward method for wide-area fault location on transmission networks," *IEEE Trans. Power Del.*, vol. 30, no. 1, pp. 264–272, Feb. 2015.

[52] O. Gmez, C. Portilla, and M. A. Ros, "Reliability analysis of substation monitoring systems based on branch PMUs," *IEEE Trans. Power Syst.*, vol. 30, no. 2, pp. 962–969, Mar. 2015.

[53] A. Monticelli and A. Garcia, "Modeling zero impedance branches in power system state estimation," *IEEE Trans. Power Syst.*, vol. 6, no. 4, pp. 1561–1570, Nov. 1991.

[54] A. Monticelli, "Modeling circuit breakers in weighted least squares state estimation," *IEEE Trans. Power Syst.*, vol. 8, no. 3, pp. 1143–1149, Aug. 1993.

[55] K. A. Clements and A. S. Costa, "Topology error identification using normalized Lagrange multipliers," *IEEE Trans. Power Syst.*, vol. 13, no. 2, pp. 347–353, May 1998.

[56] E. Lourenco, A. J. A. Costa, K. A. Clements, and R. A. Cernev, "A topology error identification method directly based on collinearity tests," *IEEE Trans. Power Syst.*, vol. 21, no. 4, pp. 1920–1929, Nov. 2006.

[57] O. Alsaç, N. Vempati, B. Stott, and A. Monticelli, "Generalized state estimation," *IEEE Trans. Power Syst.*, vol. 13, no. 3, pp. 1069–1075, Aug. 1998.

[58] A. Gómez Expósito and A. de la Villa Jaén, "Reduced substation models for generalized state estimation," *IEEE Trans. Power Syst.*, vol. 16, no. 4, pp. 839–846, Nov. 2001.

[59] A. De La Villa Jaén and A. Gómez-Expósito, "Implicitly constrained substation model for state estimation," *IEEE Trans. Power Syst.*, vol. 17, no. 3, pp. 850–856, Aug. 2002.

[60] O. Alsac, B. Stott, and W. F. Tinney, "Sparsity-oriented compensation methods for modified network solutions," *IEEE Trans. Power App. Syst.*, vol. PAS-102, no. 5, pp. 1050–1059, May 1983.

[61] W. W. Hager, "Updating the inverse of a matrix," *SIAM Rev.*, vol. 31, no. 2, pp. 221–239, Jun. 1989.

[62] R. D. Zimmerman, C. E. Murillo-Sánchez, and R. J. Thomas, "MATPOWER: Steady-state operations, planning and analysis tools for power systems research and education," *IEEE Trans. Power Syst.*, vol. 26, no. 1, pp. 12–19, Feb. 2011.

Authors' photographs and biographies not available at the time of publication.